Composite Structures 174 (2017) 176–186

Contents lists available at ScienceDirect

Composite Structures

journal homepage: www.elsevier.com/locate/compstruct

Evaluation of effective material properties in magneto-electro-elastic composite materials

Jan Sladek [a,*], Vladimir Sladek [a], Miroslav Repka [a], Jozef Kasala [b], Peter Bishay [c]

[a] Institute of Construction and Architecture, Slovak Academy of Sciences, 84503 Bratislava, Slovakia
[b] Faculty of Special Technology, University of Trencin, 91150 Trencin, Slovakia
[c] College of Engineering and Computer Science, California State University, Northridge, CA, United States

ARTICLE INFO

Article history:
Received 24 March 2017
Revised 28 March 2017
Accepted 29 March 2017
Available online 12 April 2017

Keywords:
Meshless local integral equation
Gradient theory
Size effect
Magnetoelectroelastic solid
Effective material parameters

ABSTRACT

The meshless local integral equation method is developed to analyze general two-dimensional boundary value problems in size-dependent magnetoelectroelastic solids. A consistent theory is developed for size dependent magnetoelectroelasticity. The strain gradients are considered in the constitutive equations for electric displacement and magnetic induction. The governing equations are derived with the corresponding boundary conditions using the variational principle. The local integral equations are subsequently derived and the meshless moving least square (MLS) numerical method is implemented to solve these equations.

1. Introduction

Modern smart structures made of piezoelectric and piezomagnetic materials offer certain potential performance advantages over conventional ones due to their capability of converting energy from one type to another, among magnetic, electric, and mechanical [1,2]. It is well known that some composite materials can provide superior properties compared to their virgin monolithic constituent materials [3]. The irregularity in the spatial arrangement of the fibers and their geometry can influence the estimation of the effective material properties of the unidirectional composite. The experimental approaches are not convenient for an optimal design of composites due to the expensive cost of the measurements and the low efficiency. Therefore, mathematical and numerical models are frequently utilized to get homogenized material properties directly from those of the constituents and from their microstructure. Then, these material properties are used for numerical analyses at macroscopic scale. However, sometimes such analyses are not accurate enough, especially if the size of the structure is comparable to the material length scale.

Due to their superior physical, electrical, optical, chemical and other properties, the nano/micro structures were expanded into many areas such as nano-electromechanical devices [4], space and bio-engineering [5], actuators [6], and nanocomposites [7,8]. The validity of using the classical continuum mechanics for micro/nano structures is inconclusive. Experimental as well as discrete atomistic methods such as molecular dynamics (MD) simulations [9,10] have been utilized in understanding and analysing the behaviour of nano/micro structures. However, these methods are highly expensive and not applicable to real sized structures due to the extremely high computer hardware requirements. Fortunately, the continuum theory can be applied for these structures after proper improvements or enhancements [11]. Recent experiments have demonstrated that when the dimensions of the structure are of the same order of the material length scale, the stiffness of the structure increases. Size-dependent behaviour has been observed in many studies [12–15]. This phenomenon can be explained by the presence of significant strain gradients which appear because of the small size of the microstructural elements. Thus, the behaviour of the mesoscopic structural elements could be described by the continuum theory enriched by incorporation of strain gradients. Then, a consistent size-dependent continuum mechanics theory can be a more efficient alternative to the atomistic models.

Magnetoelectroelastic (MEE) composites are made of piezoelectric and magnetostrictive phases coupled by a strain field. From

* Corresponding author.
E-mail address: jan.sladek@savba.sk (J. Sladek).

http://dx.doi.org/10.1016/j.compstruct.2017.03.104
0263-8223/

earlier investigation for macro-sized layered MEE, it is well-known that effective composite coefficients are higher than their constituents [16]. A similar enhancement of effective coefficients has been observed for fiber composites. Kuo and Wang [17] optimized the effective magnetoelectric (ME) voltage coefficient of fibrous composites made of piezoelectric and piezomagnetic phases. They showed that at an optimal orientation of fibers, the effective in-plane and out-of-plane ME coefficient can be enhanced many-fold. Wang and Pan [18] investigated the influence of imperfect matrix-fiber bond on the ME coefficient under longitudinal shear.

The influence of strain gradients in the gradient theory on the effective material properties of MEE composites, if coated piezoelectric fiber is embedded into the piezomagnetic matrix, is investigated in the present paper. This problem was analyzed before using the classical elasticity theory. Kuo [19] and Kuo and Pan [20] analyzed fibrous composites with piezoelectric and piezomagnetic phases only under anti-plane shear deformation, whereas Sladek et al. [21] analyzed the same composites under in-plane deformation. Ebrahimi and Dabbagh [22] also studied the flexural wave propagation responses of smart FG MEE nanoplates via nonlocal strain gradient theory. If the thickness of the coating layer is very small, the strain gradients should be included into the magnetoelectroelasticity mathematical model. The governing equations for magnetoelectroelastic solids in gradient elasticity with the corresponding boundary conditions are derived from the variational principle in the present paper.

Meshless methods are becoming very popular in numerical analyses of engineering problems. A variety of meshless methods has been proposed so far. They can be derived either from a weak- or strong-form. The weak formulation can be performed on the global domain or a set of local subdomains. Background cells are required in the global weak formulation to perform numerical integration. However, no background cells are required in the local weak formulation. The moving least squares (MLS) approximation is often used for approximating the trial functions. It yields C^1 continuity counterpart to conventional discretization methods, where discontinuity of secondary fields at the interfaces of elements occurs. Meshless methods have been also applied to piezoelectric problems [23,24]. Many meshless formulations can be defined on the base of the meshless local Petrov-Galerkin (MLPG) method, since trial and test functions can be chosen from different functional spaces [25–27]. The test functions in the MLPG method can be arbitrary. The formulation with a Heaviside step function as the test functions [28,29] leads to a simple form and it has been applied successfully to various boundary value problems [30–34].

In the present paper, the MLPG method, with the gradient theory, is applied to 2-D problems of magnetoelectroelasticity. The corresponding governing equations are satisfied in a weak form on small fictitious subdomains. Nodal points are randomly distributed over the analyzed domain. Each node is surrounded by a small circle for simplicity, but without loss of shape generality. Numerical integration over circles can be easily carried out. The local integral equations have a very simple nonsingular form. The MLS scheme is used for spatial approximations of the displacements, the electric and magnetic potentials [35]. Performing the spatial integrations, a system of linear algebraic equations for the unknown nodal values is obtained. The proposed computational method is applied to evaluation of effective material properties of a piezomagnetic matrix with regularly distributed piezoelectric fibers with a nano-sized coating layer. The influence of the coating layer on the effective MEE coefficients is investigated.

2. Basic equations for electric- and magnetic-strain gradient theory

The electric field-strain gradient theory for nano-dielectrics introduced by Hu and Shen [36] is extended here for a nano-magnetoelectroelastic material. The strain gradients exist only in the higher order stress, electric displacement and magnetic induction fields. Then, the constitutive equations are given by

$$\begin{aligned}
\sigma_{ij} &= c_{ijkl}\gamma_{kl} - e_{kij}E_k - q_{kij}H_k,\\
\tau_{jkl} &= -f_{ijkl}E_i - h_{ijkl}H_i + g_{jklmni}\eta_{mni},\\
D_k &= e_{kij}\gamma_{ij} + \varepsilon_{kl}E_l + \alpha_{kl}H_l + f_{klmn}\eta_{lmn},\\
B_k &= q_{kij}\gamma_{ij} + \alpha_{kl}E_l + \mu_{kl}H_l + h_{klmn}\eta_{lmn},,
\end{aligned} \tag{1}$$

where $c_{ijkl}, e_{kij}, q_{kij}, \varepsilon_{kl}, \alpha_{kl}, \mu_{kl}$ and $f_{ijkl}, h_{ijkl}, g_{jklmni}$ are the material property tensors. Particularly, $\varepsilon_{kl}, \mu_{kl}, c_{ijkl}$ are the second-order permittivity, permeability and the fourth-order elasticity constant tensors, respectively. Symbol e_{kij} denotes the piezoelectric coefficient, q_{kij} is the piezomagnetic coefficient, α_{kl} is the electromagnetic coefficient. The electric field–strain gradient coupling coefficient tensor f_{ijkl} represents the higher-order electromechanical coupling induced by the strain gradient, and h_{ijkl} is the magnetic field–strain gradient coupling coefficient tensor. The higher-order elastic parameters g_{jklmni} represent the purely the strain gradient elasticity theory. Symbols τ_{ijk} and D_i denote the higher-order stress tensor and electric displacement vector, respectively. A subscript preceded by a comma denotes differentiation with respect to the corresponding Cartesian coordinate. The Eistein summation is employed for repeated lowercase indices.

The strain tensor γ_{ij}, the electric field vector E_j and the magnetic field vector H_l are related to the displacements u_i, the electric potential ϕ and the magnetic potential ψ, respectively by

$$\gamma_{ij} = \frac{1}{2}(u_{i,j} + u_{j,i}), \quad E_j = -\phi_{,j}, \quad H_j = -\psi_{,j} \tag{2}$$

The strain gradient tensor [37] is defined as

$$\eta_{ijk} = \gamma_{ij,k} = \frac{1}{2}(u_{i,jk} + u_{j,ik}) \tag{3}$$

with exhibiting the symmetry $\gamma_{ij} = \gamma_{ji}$, $\eta_{ijk} = \eta_{jik}$. The constitutive equations (1) for orthotropic material can be written in a matrix form:

$$\begin{bmatrix}\sigma_{11}\\ \sigma_{33}\\ \sigma_{13}\end{bmatrix} = \begin{bmatrix}c_{11} & c_{13} & 0\\ c_{13} & c_{33} & 0\\ 0 & 0 & c_{44}\end{bmatrix}\begin{bmatrix}\gamma_{11}\\ \gamma_{33}\\ 2\gamma_{13}\end{bmatrix} - \begin{bmatrix}0 & e_{31}\\ 0 & e_{33}\\ e_{15} & 0\end{bmatrix}\begin{bmatrix}E_1\\ E_3\end{bmatrix} - \begin{bmatrix}0 & q_{31}\\ 0 & q_{33}\\ q_{15} & 0\end{bmatrix}\begin{bmatrix}H_1\\ H_3\end{bmatrix}$$

$$\text{or} \quad \boldsymbol{\sigma} = \mathbf{C}\boldsymbol{\gamma} - \mathbf{L}\mathbf{E} - \mathbf{M}\mathbf{H} \tag{4}$$

$$\begin{bmatrix}D_1\\ D_3\end{bmatrix} = \begin{bmatrix}0 & 0 & e_{15}\\ e_{31} & e_{33} & 0\end{bmatrix}\begin{bmatrix}\gamma_{11}\\ \gamma_{33}\\ 2\gamma_{13}\end{bmatrix} + \begin{bmatrix}\varepsilon_{11} & 0\\ 0 & \varepsilon_{33}\end{bmatrix}\begin{bmatrix}E_1\\ E_3\end{bmatrix} + \begin{bmatrix}\alpha_{11} & 0\\ 0 & \alpha_{33}\end{bmatrix}\begin{bmatrix}H_1\\ H_3\end{bmatrix} + m^2\begin{bmatrix}0 & 0 & e_{15} & 0 & 0 & e_{15}\\ e_{31} & e_{31} & 0 & e_{33} & e_{33} & 0\end{bmatrix}\begin{bmatrix}\eta_{111}\\ \eta_{331}\\ 2\eta_{131}\\ \eta_{113}\\ \eta_{333}\\ 2\eta_{133}\end{bmatrix}$$

$$\text{or} \quad \mathbf{D} = \mathbf{L}^T\boldsymbol{\gamma} + \mathbf{J}\mathbf{E} + \mathbf{A}\mathbf{H} + m^2\mathbf{F}\boldsymbol{\eta}, \tag{5}$$

$$\begin{bmatrix} B_1 \\ B_3 \end{bmatrix} = \begin{bmatrix} 0 & 0 & q_{15} \\ q_{31} & q_{33} & 0 \end{bmatrix} \begin{bmatrix} \gamma_{11} \\ \gamma_{33} \\ 2\gamma_{13} \end{bmatrix} + \begin{bmatrix} \alpha_{11} & 0 \\ 0 & \alpha_{33} \end{bmatrix} \begin{bmatrix} E_1 \\ E_3 \end{bmatrix} + \begin{bmatrix} \mu_{11} & 0 \\ 0 & \mu_{33} \end{bmatrix} \times \begin{bmatrix} H_1 \\ H_3 \end{bmatrix} + m^2 \begin{bmatrix} 0 & 0 & q_{15} & 0 & 0 & q_{15} \\ q_{31} & q_{31} & 0 & q_{33} & q_{33} & 0 \end{bmatrix} \begin{bmatrix} \eta_{111} \\ \eta_{331} \\ 2\eta_{131} \\ \eta_{113} \\ \eta_{333} \\ 2\eta_{133} \end{bmatrix}$$

$$\text{or} \quad \mathbf{B} = \mathbf{M}^T\boldsymbol{\gamma} + \mathbf{A}\mathbf{E} + \mathbf{I}\mathbf{H} + m^2\mathbf{O}\boldsymbol{\eta}, \tag{6}$$

$$\begin{bmatrix} \tau_{111} \\ \tau_{331} \\ \tau_{131} \\ \tau_{113} \\ \tau_{333} \\ \tau_{133} \end{bmatrix} = -m^2 \begin{bmatrix} 0 & e_{31} \\ 0 & e_{33} \\ e_{15} & 0 \\ 0 & e_{31} \\ 0 & e_{33} \\ e_{15} & 0 \end{bmatrix} \begin{bmatrix} E_1 \\ E_3 \end{bmatrix} - m^2 \begin{bmatrix} 0 & q_{31} \\ 0 & q_{33} \\ q_{15} & 0 \\ 0 & q_{31} \\ 0 & q_{33} \\ q_{15} & 0 \end{bmatrix} \begin{bmatrix} H_1 \\ H_3 \end{bmatrix} + l^2 \begin{bmatrix} c_{11} & c_{13} & 0 & 0 & 0 & 0 \\ c_{13} & c_{33} & 0 & 0 & 0 & 0 \\ 0 & 0 & c_{44} & 0 & 0 & 0 \\ 0 & 0 & 0 & c_{11} & c_{13} & 0 \\ 0 & 0 & 0 & c_{13} & c_{33} & 0 \\ 0 & 0 & 0 & 0 & 0 & c_{44} \end{bmatrix} \begin{bmatrix} \eta_{111} \\ \eta_{331} \\ 2\eta_{131} \\ \eta_{113} \\ \eta_{333} \\ 2\eta_{133} \end{bmatrix}$$

$$\text{or} \quad \boldsymbol{\tau} = -m^2\mathbf{F}^T\mathbf{E} - m^2\mathbf{O}^T\mathbf{H} + l^2\mathbf{G}\boldsymbol{\eta} \tag{7}$$

where gradient theory parameters g_{jklmni} are proportional to elastic parameters c_{klmn} by the internal length material parameter l [38]. Similarly, the electric field-strain gradient and magnetic field-strain gradient coupling coefficient f_{ijkl} and h_{ijkl} are expressed by piezoelectric and piezomagnetic coefficients, respectively, and a scaling parameter m.

Consider a piezoelectric solid in domain V with boundary Γ. The variation of the electric Gibbs free energy in gradient theory of magnetoelectroelastic solids is given by

$$\delta U = \int_V (\sigma_{ij}\delta\varepsilon_{ij} + \tau_{ijk}\delta\eta_{ijk} + D_k\delta\phi_{,k} + H_k\delta\psi_{,k})dV. \tag{8}$$

Applying the Gauss divergence theorem, one gets

$$\begin{aligned} \delta U &= \int_V (\sigma_{ij}\delta u_{i,j} + \tau_{ijk}\delta u_{i,jk} + D_k\delta\phi_{,k} + H_k\delta\psi_{,k})dV \\ &= -\int_V (\sigma_{ij,j}\delta u_i + \tau_{ijk,k}\delta u_{i,j} + D_{k,k}\delta\phi + H_{k,k}\delta\psi)dV \\ &\quad + \int_\Gamma (n_j\sigma_{ij}\delta u_i + n_k\tau_{ijk}\delta u_{i,j} + n_kD_k\delta\phi + n_kH_k\delta\psi)d\Gamma \\ &= -\int_V [(\sigma_{ij,j} - \tau_{ijk,jk})\delta u_i + D_{k,k}\delta\phi + H_{k,k}\delta\psi]dV \\ &\quad + \int_\Gamma [n_j(\sigma_{ij} - \tau_{ijk,k})\delta u_i + n_k\tau_{ijk}\delta u_{i,j} + n_kD_k\delta\phi + n_kH_k\delta\psi]d\Gamma \\ &= -\int_V [(\sigma_{ij,j} - \tau_{ijk,jk})\delta u_i + D_{k,k}\delta\phi + H_{k,k}\delta\psi]dV \\ &\quad + \int_\Gamma [t_i\delta u_i + R_i\delta s_i + Q\delta\phi + S\delta\psi]d\Gamma, \end{aligned} \tag{9}$$

where the traction vector is defined as

$$t_i = n_j(\sigma_{ij} - \tau_{ijk,k}) - \frac{\partial\rho_i}{\partial\boldsymbol{\pi}} + \sum_c \|\rho_i(\mathbf{x}^c)\|\delta(\mathbf{x} - \mathbf{x}^c) \tag{10}$$

with $$\rho_i := n_k\pi_j\tau_{ijk} \tag{11}$$

and $\|\rho_i(\mathbf{x}^c)\| := \rho_i(\mathbf{x}^c + 0) - \rho_i(\mathbf{x}^c - 0)$ is the jump at a corner on the oriented boundary contour Γ. Symbol π_i is the Cartesian component of the unit tangent vector on Γ, $s_i := \frac{\partial u_i}{\partial\mathbf{n}}$, $R_i := n_kn_j\tau_{ijk}$, $Q := n_kD_k$, $S := n_kH_k$.

In derivation of δU, the following identity is invoked:

$$n_k\tau_{ijk}\delta u_{i,j} = \rho_i\frac{\partial\delta u_i}{\partial\boldsymbol{\pi}} + R_i\delta\left(\frac{\partial u_i}{\partial\mathbf{n}}\right) \tag{12}$$

The primary fields (u_i, s_i, ϕ, ψ) are energetically conjugated with (t_i, R_i, Q, S). The work of the external generalized forces $(\bar{t}_i, \bar{R}_i, \bar{Q}, \bar{S})$ is given by

$$\delta W = \int_{\Gamma_t} \bar{t}_i\delta u_i d\Gamma + \int_{\Gamma_R} \bar{R}_i\delta s_i d\Gamma + \int_{\Gamma_Q} \bar{Q}\delta\phi d\Gamma + \int_{\Gamma_S} \bar{S}\delta\psi d\Gamma \tag{13}$$

From the principle of virtual work $\delta U - \delta W = 0$, the following governing equations are obtained from Eqs. (9) and (13),

$$\sigma_{ij,j}(\mathbf{x}) - \tau_{ijk,jk}(\mathbf{x}) = 0, \quad D_{k,k}(\mathbf{x}) = 0, \quad H_{k,k}(\mathbf{x}) = 0, \tag{14}$$

and two kinds of boundary conditions (b.c.) are:

$$\text{Essential b.c.}: \begin{array}{l} u_i(\mathbf{x}) = \bar{u}_i(\mathbf{x}) \text{ on } \Gamma_u, \quad \Gamma_u \subset \Gamma \\ s_i(\mathbf{x}) = \bar{s}_i(\mathbf{x}) \text{ on } \Gamma_s, \quad \Gamma_s \subset \Gamma \\ \phi(\mathbf{x}) = \bar{\phi}(\mathbf{x}) \text{ on } \Gamma_\phi, \quad \Gamma_\phi \subset \Gamma \\ \psi(\mathbf{x}) = \bar{\psi}(\mathbf{x}) \text{ on } \Gamma_\psi, \quad \Gamma_\psi \subset \Gamma \end{array} \tag{15}$$

$$\begin{array}{ll} \text{Natural b.c.}: & t_i(\mathbf{x}) = \bar{t}_i(\mathbf{x}) \text{ on } \Gamma_t, \quad \Gamma_t \cup \Gamma_u = \Gamma, \quad \Gamma_t \cap \Gamma_u = \varnothing \\ & R_i(\mathbf{x}) = \bar{R}_i(\mathbf{x}) \text{ on } \Gamma_R, \quad \Gamma_R \cup \Gamma_s = \Gamma, \quad \Gamma_R \cup \Gamma_s = \varnothing \\ & Q(\mathbf{x}) = \bar{Q}(\mathbf{x}) \text{ on } \Gamma_Q, \quad \Gamma_Q \cup \Gamma_\phi = \Gamma, \quad \Gamma_Q \cup \Gamma_\phi = \varnothing \\ & S(\mathbf{x}) = \bar{S}(\mathbf{x}) \text{ on } \Gamma_S, \quad \Gamma_S \cup \Gamma_\psi = \Gamma, \quad \Gamma_S \cup \Gamma_\psi = \varnothing \end{array} \tag{16}$$

3. The meshless local integral equation method

The MLPG method is the local weak-form with local fictitious subdomains Ω_s. It is a small region constructed for each node inside the global domain [27,35]. The shape of local subdomains could be of any geometry and size. In the present paper, the local subdomains are circular for numerical simplicity. The local weak-form of the first governing equation (14) can be written as

$$\int_{\Omega_s} [\sigma_{ij,j}(\mathbf{x}) - \tau_{ijk,jk}(\mathbf{x})]\, u^*_{ik}(\mathbf{x})\, d\Omega = 0 \tag{17}$$

where $u^*_{ik}(\mathbf{x})$ is a test function.

Applying the Gauss divergence theorem to the weak-form (17) one obtains

$$\int_{\partial\Omega_s} [\sigma_{ij}(\mathbf{x}) - \tau_{ijk,k}(\mathbf{x})]n_j(\mathbf{x})u^*_{ik}(\mathbf{x})d\Gamma - \int_{\Omega_s} [\sigma_{ij}(\mathbf{x}) - \tau_{ijk,k}(\mathbf{x})]u^*_{ik,j}(\mathbf{x})d\Omega = 0, \tag{18}$$

where $\partial\Omega_s$ is the boundary of the local subdomain. It consists of three parts $\partial\Omega_s = L_s \cup \Gamma_{st} \cup \Gamma_{su}$ [35], where L_s is the local boundary that is totally inside the global domain, Γ_{st} is the part of the local boundary which coincides with the global boundary with prescribed tractions, i.e., $\Gamma_{st} = \partial\Omega_s \cap \Gamma_t$, and similarly Γ_{su} is the part of the local boundary with prescribed displacements, i.e., $\Gamma_{su} = \partial\Omega_s \cap \Gamma_u$.

If a Heaviside step function is chosen as the test function $u^*_{ik}(\mathbf{x})$ in each subdomain as

$$u^*_{ik}(\mathbf{x}) = \begin{cases} \delta_{ik} & \text{at} \quad \mathbf{x} \in \Omega_s \\ 0 & \text{at} \quad \mathbf{x} \notin \Omega_s \end{cases}, \tag{19}$$

the local weak-form (18) is transformed into the following local boundary-domain integral equations

$$\int_{L_s+\Gamma_{su}} n_j(\sigma_{ij} - \tau_{ijk,k})d\Gamma + \rho_i(\mathbf{x}^f_{st}) - \rho_i(\mathbf{x}^s_{st}) = -\int_{\Gamma_{st}} \bar{t}_i d\Gamma, \tag{20}$$

where definition of the traction vector (10) is utilized and $\mathbf{x}_{st}^{f}$, $\mathbf{x}_{st}^{s}$ stand for the final and starting points on Γ_{st}.

Similarly, the local weak-form of the second governing equation (14) can be written as

$$\int_{\Omega_s} D_{k,k}(\mathbf{x})\, v^*(\mathbf{x})\, d\Omega = 0, \tag{21}$$

where $v^*(\mathbf{x})$ is a test function.

Applying the Gauss divergence theorem to Eq. (21) and choosing the Heaviside step function as the test function $v^*(\mathbf{x})$ one can obtain

$$\int_{L_s+\Gamma_{s\phi}} Q(\mathbf{x})d\Gamma = -\int_{\Gamma_{sQ}} \bar{Q}(\mathbf{x})d\Gamma, \tag{22}$$

where

$$Q(\mathbf{x}) = D_k(\mathbf{x})n_k(\mathbf{x}) = \left[e_{kij}u_{i,j}(\mathbf{x}) - \varepsilon_{kl}\phi_{,l}(\mathbf{x}) - \alpha_{kl}\psi_{,l}(\mathbf{x}) + f_{klmn}u_{l,mn}(\mathbf{x})\right]n_k. \tag{23}$$

The local integral equation corresponding to the third governing equation (14) has the form

$$\int_{L_s+\Gamma_{s\psi}} S(\mathbf{x})d\Gamma = -\int_{\Gamma_{sS}} \bar{S}(\mathbf{x})d\Gamma, \tag{24}$$

where magnetic flux is given by

$$S(\mathbf{x}) = B_k(\mathbf{x})n_k(\mathbf{x}) = \left[q_{kij}u_{i,j}(\mathbf{x}) - \alpha_{kl}\phi_{,l}(\mathbf{x}) - \mu_{kl}\psi_{,l}(\mathbf{x}) + h_{klmn}u_{l,mn}(\mathbf{x})\right]n_j. \tag{25}$$

In the MLPG method the test and the trial functions can be from different functional spaces. The MLS approximation is used for approximation of trial functions. A number of nodes is spread over the domain of influence. The approximated functions for primary fields (mechanical displacements, electric and magnetic potentials) are given by [33]

$$\mathbf{u}^h(\mathbf{x}) = \mathbf{N}^T(\mathbf{x})\cdot\hat{\mathbf{u}} = \sum_{a=1}^{n} N^a(\mathbf{x})\hat{\mathbf{u}}^a, \quad \phi^h(\mathbf{x}) = \sum_{a=1}^{n} N^a(\mathbf{x})\hat{\phi}^a,$$
$$\psi^h(\mathbf{x}) = \sum_{a=1}^{n} N^a(\mathbf{x})\hat{\psi}^a \tag{26}$$

where the nodal values $\hat{\mathbf{u}}^a = (\hat{u}_1^a, \hat{u}_3^a)^T$, $\hat{\phi}^a$ and $\hat{\psi}^a$ are fictitious parameters for displacements, electric and magnetic potentials, respectively, and $N^a(\mathbf{x})$ is the shape function related to the node a. The number of nodes n used for the approximation is determined by the weight function $w^a(\mathbf{x})$. The forth-order spline-type weight function is applied in the present work

$$w^a(\mathbf{x}) = \begin{cases} 1 - 6\left(\frac{d^a}{r^a}\right)^2 + 8\left(\frac{d^a}{r^a}\right)^3 - 3\left(\frac{d^a}{r^a}\right)^4, & 0 \leqslant d^a \leqslant r^a \\ 0, & d^a \geqslant r^a \end{cases} \tag{27}$$

where $d^a = \|\mathbf{x} - \mathbf{x}^a\|$ and r^a is the size of the support domain. This weight function has the C^1- continuity over the entire domain, and therefore the continuity conditions of tractions, electric charge and magnetic flux are satisfied.

The traction vector $t_i(\mathbf{x})$ at a boundary point $\mathbf{x} \in \partial\Omega_s$ can be easily approximated in terms of primary fields as

$$\begin{aligned}\mathbf{t}^h(\mathbf{x}) = {} & \mathbf{N}(\mathbf{x})\mathbf{C}\sum_{a=1}^{n}\mathbf{B}^a(\mathbf{x})\hat{\mathbf{u}}^a + \mathbf{N}(\mathbf{x})\mathbf{L}\sum_{a=1}^{n}\mathbf{P}^a(\mathbf{x})\hat{\phi}^a + \mathbf{N}(\mathbf{x})\mathbf{M}\sum_{a=1}^{n}\mathbf{P}^a(\mathbf{x})\hat{\psi}^a \\ & - m^2\mathbf{N}(\mathbf{x})\mathbf{L}\sum_{a=1}^{n}\mathbf{P}_1^a(\mathbf{x})\hat{\phi}^a - m^2\mathbf{N}(\mathbf{x})\mathbf{L}\sum_{a=1}^{n}\mathbf{P}_3^a(\mathbf{x})\hat{\phi}^a \\ & - m^2\mathbf{N}(\mathbf{x})\mathbf{M}\sum_{a=1}^{n}\mathbf{P}_1^a(\mathbf{x})\hat{\psi}^a - m^2\mathbf{N}(\mathbf{x})\mathbf{M}\sum_{a=1}^{n}\mathbf{P}_3^a(\mathbf{x})\hat{\psi}^a \\ & + l^2\mathbf{N}(\mathbf{x})\mathbf{C}\sum_{a=1}^{n}\mathbf{B}_1^a(\mathbf{x})\mathbf{u}^a + l^2\mathbf{N}(\mathbf{x})\mathbf{C}\sum_{a=1}^{n}\mathbf{B}_3^a(\mathbf{x})\mathbf{u}^a,\end{aligned} \tag{28}$$

where the matrices $\mathbf{C}$, $\mathbf{L}$, and $\mathbf{M}$ are defined in Eq. (4), the matrix $\mathbf{N}(\mathbf{x})$ is related to the normal vector $\mathbf{n}(\mathbf{x})$ on $\partial\Omega_s$ by

$$\mathbf{N}(\mathbf{x}) = \begin{bmatrix} n_1 & 0 & n_3 \\ 0 & n_3 & n_1 \end{bmatrix} \tag{29}$$

and finally, the matrices $\mathbf{B}^a$ and $\mathbf{P}^a$ are represented by the gradients of the shape functions as

$$\mathbf{B}^a(\mathbf{x}) = \begin{bmatrix} N^a_{,1} & 0 \\ 0 & N^a_{,3} \\ N^a_{,3} & N^a_{,1} \end{bmatrix}, \quad \mathbf{B}_{1a}(\mathbf{x}) = \begin{bmatrix} N^a_{,111} & 0 \\ 0 & N^a_{,311} \\ N^a_{,311} & N^a_{,111} \end{bmatrix},$$
$$\mathbf{B}_{3a}(\mathbf{x}) = \begin{bmatrix} N^a_{,133} & 0 \\ 0 & N^a_{,333} \\ N^a_{,333} & N^a_{,133} \end{bmatrix},$$
$$\mathbf{P}^a(\mathbf{x}) = \begin{bmatrix} N^a_{,1} \\ N^a_{,3} \end{bmatrix}, \quad \mathbf{P}_{1a}(\mathbf{x}) = \begin{bmatrix} N^a_{,111} \\ N^a_{,311} \end{bmatrix}, \quad \mathbf{P}_{3a}(\mathbf{x}) = \begin{bmatrix} N^a_{,133} \\ N^a_{,333} \end{bmatrix}. \tag{30}$$

Similarly, the normal component of the electric displacement vector $Q(\mathbf{x})$ can be approximated by

$$\begin{aligned} Q^h(\mathbf{x}) = {} & \mathbf{N}_1(\mathbf{x})\mathbf{L}^T\sum_{a=1}^{n}\mathbf{B}^a(\mathbf{x})\hat{\mathbf{u}}^a - \mathbf{N}_1(\mathbf{x})\mathbf{J}\sum_{a=1}^{n}\mathbf{P}^a(\mathbf{x})\hat{\phi}^a \\ & - \mathbf{N}_1(\mathbf{x})\mathbf{A}\sum_{a=1}^{n}\mathbf{P}^a(\mathbf{x})\hat{\psi}^a + m^2\mathbf{N}_1(\mathbf{x})\mathbf{L}^T\sum_{a=1}^{n}\mathbf{B}_4^a(\mathbf{x})\hat{\mathbf{u}}^a \\ & + m^2\mathbf{N}_1(\mathbf{x})\mathbf{L}^T\sum_{a=1}^{n}\mathbf{B}_5^a(\mathbf{x})\hat{\mathbf{u}}^a, \end{aligned} \tag{31}$$

where the matrices $\mathbf{L}^{\mathbf{T}}$, $\mathbf{J}$, and $\mathbf{A}$ are defined in Eq. (5) and

$$\mathbf{N}_1(\mathbf{x}) = [\,n_1 \quad n_3\,], \quad \mathbf{B}_4^a(\mathbf{x}) = \begin{bmatrix} N^a_{,11} & 0 \\ 0 & N^a_{,31} \\ N^a_{,31} & N^a_{,11} \end{bmatrix}, \quad \mathbf{B}_5^a(\mathbf{x}) = \begin{bmatrix} N^a_{,13} & 0 \\ 0 & N^a_{,33} \\ N^a_{,33} & N^a_{,13} \end{bmatrix}. \tag{32}$$

The magnetic flux $S(\mathbf{x})$ is approximated by

$$\begin{aligned} S^h(\mathbf{x}) = {} & \mathbf{N}_1(\mathbf{x})\mathbf{M}^{\mathbf{T}}\sum_{a=1}^{n}\mathbf{B}^a(\mathbf{x})\hat{\mathbf{u}}^a - \mathbf{N}_1(\mathbf{x})\mathbf{A}\sum_{a=1}^{n}\mathbf{P}^a(\mathbf{x})\hat{\phi}^a \\ & - \mathbf{N}_1(\mathbf{x})\mathbf{I}\sum_{a=1}^{n}\mathbf{P}^a(\mathbf{x})\hat{\psi}^a + m^2\mathbf{N}_1(\mathbf{x})\mathbf{M}^{\mathbf{T}}\sum_{a=1}^{n}\mathbf{B}_4^a(\mathbf{x})\hat{\mathbf{u}}^a \\ & + m^2\mathbf{N}_1(\mathbf{x})\mathbf{M}^{\mathbf{T}}\sum_{a=1}^{n}\mathbf{B}_5^a(\mathbf{x})\hat{\mathbf{u}}^a, \end{aligned} \tag{33}$$

with the matrices $\mathbf{M}^{\mathbf{T}}$ and $\mathbf{I}$ being defined in Eq. (6).

The essential boundary conditions are satisfied in the strong-form at nodal points. One obtains the discretized form of these boundary conditions from the approximation formula (26)

$$\sum_{a=1}^{n} N^a(\zeta)\hat{\mathbf{u}}^a = \bar{\mathbf{u}}(\zeta) \quad \text{for } \zeta \in \Gamma_u, \quad \sum_{a=1}^{n}\mathbf{P}^a(\zeta)\mathbf{N}_1(\zeta)\hat{\mathbf{u}}^a = \bar{\mathbf{s}}(\zeta) \quad \text{for } \zeta \in \Gamma_s$$
$$\sum_{a=1}^{n} N^a(\zeta)\hat{\phi}^a = \bar{\phi}(\zeta) \quad \text{for } \zeta \in \Gamma_\phi, \quad \sum_{a=1}^{n} N^a(\zeta)\hat{\psi}^a = \bar{\psi}(\zeta) \quad \text{for } \zeta \in \Gamma_\psi \tag{34}$$

Substituting the MLS-approximation (28), (31), (33) into the local boundary-domain integral equations (20), (22) and (24), we obtain the system of algebraic equations for unknown nodal quantities

$$\sum_{a=1}^{n}\left(\int_{L_s+\Gamma_{st}}\mathbf{N}(\mathbf{x})\mathbf{C}\mathbf{B}^a(\mathbf{x})d\Gamma+\int_{L_s+\Gamma_{st}}l^2\mathbf{N}(\mathbf{x})\mathbf{C}(\mathbf{B}_1^a(\mathbf{x})+\mathbf{B}_3^a(\mathbf{x}))d\Gamma\right)\hat{\mathbf{u}}^a$$
$$+\sum_{a=1}^{n}\left(\int_{L_s+\Gamma_{sQ}}\mathbf{N}(\mathbf{x})\mathbf{L}\mathbf{P}^a(\mathbf{x})d\Gamma-\int_{L_s+\Gamma_{sQ}}m^2\mathbf{N}(\mathbf{x})\mathbf{L}(\mathbf{P}_1^a(\mathbf{x})+\mathbf{P}_3^a(\mathbf{x}))d\Gamma\right)\hat{\phi}^a$$
$$+\sum_{a=1}^{n}\left(\int_{L_s+\Gamma_{sS}}\mathbf{N}(\mathbf{x})\mathbf{M}\mathbf{P}^a(\mathbf{x})d\Gamma-\int_{L_s+\Gamma_{sS}}\mathbf{N}(\mathbf{x})\mathbf{M}(\mathbf{P}_1^a(\mathbf{x})+\mathbf{P}_3^a(\mathbf{x}))d\Gamma\right)\hat{\psi}^a$$
$$+l^2\left\{\mathbf{\Pi}(\mathbf{x}_{st}^f)\mathbf{C}\left[n_1\mathbf{B}_4^a(\mathbf{x}_{st}^f)+n_3\mathbf{B}_5^a(\mathbf{x}_{st}^f)\right]-\mathbf{\Pi}(\mathbf{x}_{st}^s)\mathbf{C}\left[n_1\mathbf{B}_4^a(\mathbf{x}_{st}^s)+n_3\mathbf{B}_5^a(\mathbf{x}_{st}^s)\right]\right\}\hat{\mathbf{u}}^a$$
$$=-\int_{\Gamma_{st}}\bar{\mathbf{t}}(\mathbf{x})d\Gamma, \tag{35}$$

$$\sum_{a=1}^{n}\left(\int_{L_s+\Gamma_{sQ}}\mathbf{N}_1(\mathbf{x})\mathbf{L}^T\mathbf{B}^a(\mathbf{x})d\Gamma+\int_{L_s+\Gamma_{sQ}}m^2\mathbf{N}_1(\mathbf{x})\mathbf{L}^T\mathbf{B}_4^a(\mathbf{x})d\Gamma\right.$$
$$\left.+\int_{L_s+\Gamma_{sQ}}m^2\mathbf{N}_1(\mathbf{x})\mathbf{L}^T\mathbf{B}_5^a(\mathbf{x})d\Gamma\right)\hat{\mathbf{u}}^a--\sum_{a=1}^{n}\left(\int_{L_s+\Gamma_{sQ}}\mathbf{N}_1(\mathbf{x})\mathbf{J}\mathbf{P}^a(\mathbf{x})d\Gamma\right)\hat{\phi}^a$$
$$-\sum_{a=1}^{n}\left(\int_{L_s+\Gamma_{sS}}\mathbf{N}_1(\mathbf{x})\mathbf{A}\mathbf{P}^a(\mathbf{x})d\Gamma\right)\hat{\psi}^a=-\int_{\Gamma_{sQ}}\bar{Q}(\mathbf{x})d\Gamma, \tag{36}$$

$$\sum_{a=1}^{n}\left(\int_{L_s+\Gamma_{sS}}\mathbf{N}_1(\mathbf{x})\mathbf{M}^T\mathbf{B}^a(\mathbf{x})d\Gamma+\int_{L_s+\Gamma_{sS}}\mathbf{N}_1(\mathbf{x})\mathbf{M}^T\mathbf{B}_4^a(\mathbf{x})d\Gamma\right.$$
$$\left.+\int_{L_s+\Gamma_{sS}}\mathbf{N}_1(\mathbf{x})\mathbf{M}^T\mathbf{B}_5^a(\mathbf{x})d\Gamma\right)\hat{\mathbf{u}}^a--\sum_{a=1}^{n}\left(\int_{L_s+\Gamma_{sQ}}\mathbf{N}_1(\mathbf{x})\mathbf{A}\mathbf{P}^a(\mathbf{x})d\Gamma\right)\hat{\phi}^a$$
$$-\sum_{a=1}^{n}\left(\int_{L_s+\Gamma_{sS}}\mathbf{N}_1(\mathbf{x})\mathbf{I}\mathbf{P}^a(\mathbf{x})d\Gamma\right)\hat{\psi}^a=-\int_{\Gamma_{sS}}\bar{S}(\mathbf{x})d\Gamma, \tag{37}$$

which are considered on the sub-domains adjacent to the interior nodes as well as to the boundary nodes on Γ_{st}, Γ_{sQ} and Γ_{sS} and

$$\mathbf{\Pi}(\mathbf{x})=\begin{bmatrix}\pi_1 & 0 & \pi_3\\ 0 & \pi_3 & \pi_1\end{bmatrix}. \tag{38}$$

4. Coated circular piezoelectric fiber in piezomagnetic matrix

The proposed computational method is applied for evaluating the effective material parameters of a piezomagnetic matrix with regularly distributed piezoelectric fibers of a circular cross section. The fibers are coated by a general MEE material with thickness h. The thickness of the cladding layer is considered so small that it is necessary to apply the gradient theory to describe the size effect. In idealized assessments of the effective elastic properties of unidirectionally reinforced composites, it is assumed that the spatial arrangement of fibers is regular, which enables the application of effective elasticity estimates that are usually developed by modelling the mechanics of a representative volume element (RVE). Then, it is sufficient to consider only one fiber in the square domain ($a\times a$) as the RVE (Fig. 1). The polarization in our numerical analyses is considered in the transverse direction, x_3-axis.

The effective material coefficients of MEE solids are computed from the constitutive equations (4)–(6) rewritten for the average values of the secondary fields and the average values of conjugated fields. These fields are obtained from the numerical solution of properly selected boundary value problems in the RVE sample. Let us consider a rectangular RVE sample $\Omega=\{\forall\mathbf{x}=(x_1,x_3);\ x_1\in[0,a],\ x_3\in[0,a]\}$. The volume average stress, electric displacement and magnetic induction are, respectively

$$\langle\sigma_{ij}\rangle=\frac{1}{a^2}\int_\Omega\sigma_{ij}d\Omega;\quad\langle D_i\rangle=\frac{1}{a^2}\int_\Omega D_i d\Omega;\quad\langle B_i\rangle=\frac{1}{a^2}\int_\Omega B_i d\Omega. \tag{39}$$

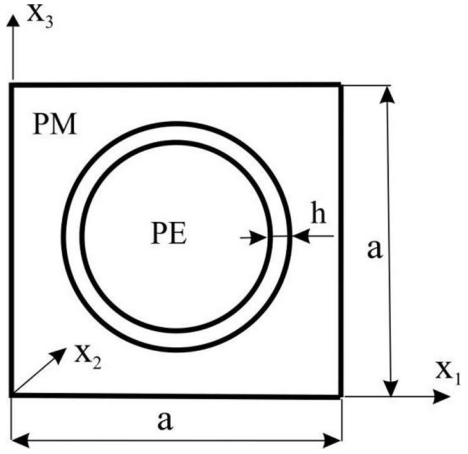

Fig. 1. Representative volume element (RVE) with piezomagnetic phase as matrix and piezoelectric phase as embedded fiber with a nano-sized coating layer of thickness h.

If a uniform strain along x_1 and vanishing electric and magnetic potentials are considered as shown in Fig. 2, we get the following average values of the secondary fields

$$\langle\gamma_{11}\rangle=\bar{\gamma}_{11}=const,\quad\langle\gamma_{33}\rangle=0,\quad\langle\gamma_{13}\rangle=0,\quad\langle E_i\rangle=0,\quad\langle H_i\rangle=0,$$
$$\langle\eta_{ijk}\rangle=0 \tag{40}$$

Then, the effective material coefficients are given by

$$c_{11}^{eff}=\frac{\langle\sigma_{11}\rangle}{\bar{\gamma}_{11}},\quad c_{13}^{eff}=\frac{\langle\sigma_{33}\rangle}{\bar{\gamma}_{11}},\quad e_{31}^{eff}=\frac{\langle D_3\rangle}{\bar{\gamma}_{11}},\quad q_{31}^{eff}=\frac{\langle B_3\rangle}{\bar{\gamma}_{11}}. \tag{41}$$

The following effective material coefficients can also be computed as

$$c_{33}^{eff}=\frac{\langle\sigma_{33}\rangle}{\bar{\gamma}_{11}},\quad c_{13}^{eff}=\frac{\langle\sigma_{11}\rangle}{\bar{\gamma}_{33}},\quad e_{33}^{eff}=\frac{\langle D_3\rangle}{\bar{\gamma}_{33}},\quad q_{33}^{eff}=\frac{\langle B_3\rangle}{\bar{\gamma}_{33}}, \tag{42}$$

if we consider a uniform strain along x_3 and vanishing electric and magnetic potentials

$$\langle\gamma_{11}\rangle=0,\quad\langle\gamma_{33}\rangle=\bar{\gamma}_{33}=const,\quad\langle\gamma_{13}\rangle=0,\quad\langle E_i\rangle=0,\quad\langle H_i\rangle=0,$$
$$\langle\eta_{ijk}\rangle=0 \tag{43}$$

Similarly, one can select the average values of the secondary fields

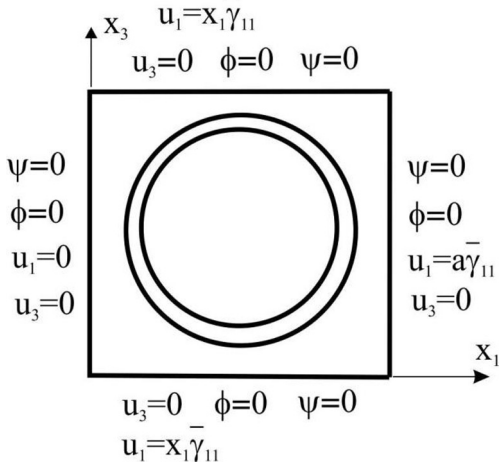

Fig. 2. Boundary conditions appropriate for evaluation of c_{11}^{eff}, c_{13}^{eff}, e_{31}^{eff}, q_{31}^{eff}.

$$\langle\gamma_{11}\rangle = 0, \quad \langle\gamma_{33}\rangle = 0, \quad \langle\gamma_{13}\rangle = \bar{\gamma}_{13} = const, \quad \langle E_i\rangle = 0, \quad \langle H_i\rangle = 0, \quad \langle\eta_{ijk}\rangle = 0 \tag{44}$$

to compute effective material coefficients

$$c_{66}^{eff} = \frac{\langle\sigma_{13}\rangle}{2\bar{\gamma}_{13}}, \quad e_{15}^{eff} = \frac{\langle D_1\rangle}{2\bar{\gamma}_{13}}, \quad q_{15}^{eff} = \frac{\langle B_1\rangle}{2\bar{\gamma}_{13}}. \tag{45}$$

If a uniform electric intensity field along x_3 and vanishing displacements are considered, the average values of the secondary fields are given as

$$\langle\gamma_{11}\rangle = 0, \quad \langle\gamma_{33}\rangle = 0, \quad \langle\gamma_{13}\rangle = 0, \quad \langle E_i\rangle = \bar{E}_3\delta_{i3} = const, \quad \langle H_i\rangle = 0, \quad \langle\eta_{ijk}\rangle = 0 \tag{46}$$

Then, one can calculate the following effective material coefficients

$$e_{31}^{eff} = -\frac{\langle\sigma_{11}\rangle}{\bar{E}_3}, \quad e_{33}^{eff} = -\frac{\langle\sigma_{33}\rangle}{\bar{E}_3}, \quad \varepsilon_{33}^{eff} = \frac{\langle D_3\rangle}{\bar{E}_3}, \quad \alpha_{33}^{eff} = \frac{\langle B_3\rangle}{\bar{E}_3}. \tag{47}$$

Similarly, a uniform electric intensity field along x_1 and vanishing displacements are considered

$$\langle\gamma_{11}\rangle = 0, \quad \langle\gamma_{33}\rangle = 0, \quad \langle\gamma_{13}\rangle = 0, \quad \langle E_i\rangle = \bar{E}_1\delta_{i1} = const, \quad \langle H_i\rangle = 0, \quad \langle\eta_{ijk}\rangle = 0 \tag{48}$$

for evaluating the effective material coefficients

$$\varepsilon_{11}^{eff} = \frac{\langle D_1\rangle}{\bar{E}_1}, \quad e_{15}^{eff} = -\frac{\langle\sigma_{13}\rangle}{\bar{E}_1}, \quad \alpha_{11}^{eff} = \frac{\langle B_1\rangle}{\bar{E}_1}. \tag{49}$$

If the following boundary conditions are considered

$$\langle\gamma_{11}\rangle = 0, \quad \langle\gamma_{33}\rangle = 0, \quad \langle\gamma_{13}\rangle = 0, \quad \langle E_i\rangle = 0, \quad \langle H_i\rangle = \bar{H}_1\delta_{i1} = const, \quad \langle\eta_{ijk}\rangle = 0 \tag{50}$$

the effective material coefficients are computed as

$$q_{15}^{eff} = -\frac{\langle\sigma_{13}\rangle}{\bar{H}_1}, \quad \alpha_{11}^{eff} = \frac{\langle D_1\rangle}{\bar{H}_1}, \quad \mu_{11}^{eff} = \frac{\langle B_1\rangle}{\bar{H}_1}. \tag{51}$$

Finally, if the average values of the secondary fields are considered as

$$\langle\gamma_{11}\rangle = 0, \quad \langle\gamma_{33}\rangle = 0, \quad \langle\gamma_{13}\rangle = 0, \quad \langle E_i\rangle = 0, \quad \langle H_i\rangle = \bar{H}_3\delta_{i3} = const, \quad \langle\eta_{ijk}\rangle = 0 \tag{52}$$

then, we can calculate the following effective material coefficients

$$q_{31}^{eff} = -\frac{\langle\sigma_{11}\rangle}{\bar{H}_3}, \quad q_{33}^{eff} = -\frac{\langle\sigma_{33}\rangle}{\bar{H}_3}, \quad \alpha_{33}^{eff} = \frac{\langle D_3\rangle}{\bar{H}_3}, \quad \mu_{33}^{eff} = \frac{\langle B_3\rangle}{\bar{H}_3}. \tag{53}$$

where the volume average values of the conjugated fields $\langle\sigma_{11}\rangle$, $\langle\sigma_{33}\rangle$, $\langle\sigma_{13}\rangle$, $\langle D_3\rangle$, $\langle B_3\rangle$ are calculated from Eq. (39), with the integrands being obtained from the solution of the considered boundary value problem.

5. Numerical examples

In the numerical examples, the RVE has a piezoelectric fiber with circular cross section in the square domain ($a \times a$). The fiber is coated by the piezomagnetic material Terfenol-D. The matrix material parameter is $CoFe_2O_4$ whose properties are given in [39]. The piezoelectric fiber is $BaTiO_3$ with parameters

$$c_{11} = 16.6 \times 10^{10}\ \mathrm{Nm}^{-2}, \quad c_{13} = 7.8 \times 10^{10}\ \mathrm{Nm}^{-2},$$
$$c_{33} = 16.2 \times 10^{10}\ \mathrm{Nm}^{-2}, \quad c_{44} = 4.3 \times 10^{10}\ \mathrm{Nm}^{-2},$$

$$e_{15} = 11.6\ \mathrm{Cm}^{-2}, \quad e_{31} = -4.4\ \mathrm{Cm}^{-2}, \quad e_{33} = 18.6\ \mathrm{Cm}^{-2},$$

$$\varepsilon_{11} = 11.2 \times 10^{-9}\ \mathrm{C}^2/\mathrm{Nm}^2, \quad \varepsilon_{33} = 12.6 \times 10^{-9}\ \mathrm{C}^2/\mathrm{Nm}^2,$$

$$q_{15} = 0.0\ \mathrm{N/Am}, \quad q_{31} = 0.0\ \mathrm{N/Am}, \quad q_{33} = 0.0\ \mathrm{N/Am},$$

$$\alpha_{11} = 0.0\ \mathrm{Ns/VC}, \quad \alpha_{33} = 0.0\ \mathrm{Ns/VC},$$

$$\mu_{11} = 5.0 \times 10^{-6}\ \mathrm{Ns}^2\ \mathrm{C}^{-2}, \quad \mu_{33} = 10.0 \times 10^{-6}\ \mathrm{Ns}^2\ \mathrm{C}^{-2}.$$

The piezomagnetic material Terfenol-D has the following material coefficients:

$$c_{11} = 0.854 \times 10^{10}\ \mathrm{Nm}^{-2}, \quad c_{13} = 0.391 \times 10^{10}\ \mathrm{Nm}^{-2},$$
$$c_{33} = 2.83 \times 10^{10}\ \mathrm{Nm}^{-2}, \quad c_{44} = 0.555 \times 10^{10}\ \mathrm{Nm}^{-2},$$

$$e_{15} = 0.0\ \mathrm{Cm}^{-2}, \quad e_{31} = 0.0\ \mathrm{Cm}^{-2}, \quad e_{33} = 0.0\ \mathrm{Cm}^{-2},$$

$$\varepsilon_{11} = 0.05 \times 10^{-9}\ \mathrm{C}^2/\mathrm{Nm}^2, \quad \varepsilon_{33} = 0.05 \times 10^{-9}\ \mathrm{C}^2/\mathrm{Nm}^2,$$

$$q_{15} = 155.5\ \mathrm{N/Am}, \quad q_{31} = -5.75\ \mathrm{N/Am}, \quad q_{33} = 270.1\ \mathrm{N/Am},$$

$$\alpha_{11} = 0.0\ \mathrm{Ns/VC}, \quad \alpha_{33} = 0.0\ \mathrm{Ns/VC},$$

$$\mu_{11} = 8.6 \times 10^{-6}\ \mathrm{Ns}^2\ \mathrm{C}^{-2}, \quad \mu_{33} = 2.3 \times 10^{-6}\ \mathrm{Ns}^2\ \mathrm{C}^{-2}.$$

The volume fraction of the fiber is introduced here as $f = \pi r^2/a^2$, with $r = r_0 + h$ where r_0 is the radius of the circular cross section of the fiber and h is the coating layer thickness. The following geometrical dimensions have been considered in the numerical model: $h = 1 \cdot 10^{-8}$ m and $a = 5 \cdot 10^{-7}$m.

The coating layer thickness is kept constant for all the considered volume fractions. Due to the symmetry of the problem with respect to both Cartesian coordinates, only a quarter of the RVE is modelled. We have used 300 nodes for the MLS approximation of the physical quantities in the fiber and 2414 nodes in the matrix. The quarter of the coating layer is approximated by 90 nodes. The local subdomains are assumed circular.

Now, it is needed to ensure a jump of secondary fields on interfaces. It is well known that the C^1- continuity is ensured over the entire domain in the MLS approximation. Therefore the continuity conditions of the tractions, electric displacement and magnetic induction are satisfied on interfaces too. However, this highly continuous nature leads to difficulties when there is an imposed discontinuity in the secondary fields. To simulate jumps on interfaces Krongauz and Belytschko [40] introduced a jump shape function for 2-D problems. It is a trial function with a pre-imposed discontinuity in the gradient of the function on interfaces. It is very tedious to applied this approach for curvilinear interfaces. Cordes and Moran [41] solved also 2-D problems using Lagrangian multiplier. The method requires a lot of computational effort for the discontinuity of a complex geometrical shape.

It is much simpler to apply double nodes approach for the material discontinuity [42]. Two sets of collocation nodes are assigned on both the +side and the −side of the material interface at the same location (Fig. 3). The MLS approximations are carried out separately on particular sets of nodes related to the homogeneous domains. Then, the support domains for the weights in the weighted MLS approximations must be truncated at the interface of the two media. Then, the high order continuity is kept within each homogeneous part, but not across their interface. The local subdomains considered around nodes should not cross the interface too.

On the interface Γ_I, we must enforce the continuity for the displacements and potentials, as well as the equilibrium of tractions, electric charge and magnetic flux by collocating the following equations at double nodes $\mathbf{x}^d \in \partial\Omega_s^d \cap \Gamma_I = \Gamma_I^d$:

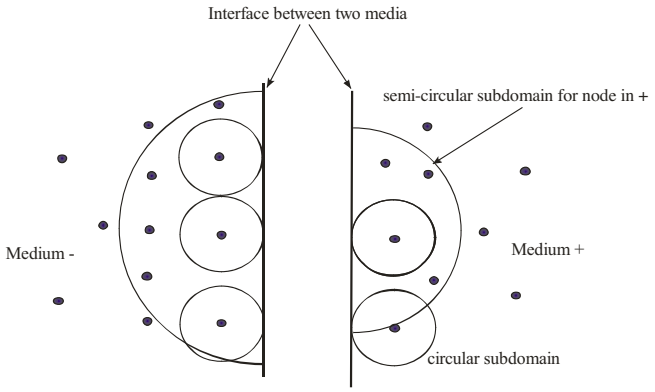

Fig. 3. Double nodes approach for material discontinuities.

$$\sum_{a=1}^{n^+} N^a(\mathbf{x}^d)\hat{\mathbf{u}}^a = \sum_{a=1}^{n^-} N^a(\mathbf{x}^d)\hat{\mathbf{u}}^a, \tag{54}$$

$$\sum_{a=1}^{n^+} N^a(\mathbf{x}^d)\hat{\phi}^a = \sum_{a=1}^{n^-} N^a(\mathbf{x}^d)\hat{\phi}^a, \tag{55}$$

$$\sum_{a=1}^{n^+} N^a(\mathbf{x}^d)\hat{\psi}^a = \sum_{a=1}^{n^-} N^a(\mathbf{x}^d)\hat{\psi}^a, \tag{56}$$

$$\begin{aligned}
\mathbf{N}(\mathbf{x}^d)\Bigg[&\mathbf{C}^+(\mathbf{x}^d)\sum_{a=1}^{n^+}\mathbf{B}^a(\mathbf{x})\hat{\mathbf{u}}^a - \mathbf{C}^-(\mathbf{x}^d)\sum_{a=1}^{n^-}\mathbf{B}^a(\mathbf{x})\hat{\mathbf{u}}^a + \mathbf{L}^+(\mathbf{x}^d)\sum_{a=1}^{n^+}\mathbf{P}^a(\mathbf{x})\hat{\phi}^a\\
&-\mathbf{L}^-(\mathbf{x}^d)\sum_{a=1}^{n^-}\mathbf{P}^a(\mathbf{x})\hat{\phi}^a + \mathbf{M}^+(\mathbf{x}^d)\sum_{a=1}^{n^+}\mathbf{P}^a(\mathbf{x})\hat{\psi}^a - \mathbf{M}^-(\mathbf{x}^d)\sum_{a=1}^{n^-}\mathbf{P}^a(\mathbf{x})\hat{\psi}^a\\
&- m^2\mathbf{L}^+(\mathbf{x}^d)\sum_{a=1}^{n^+}\mathbf{P}_1^a(\mathbf{x})\hat{\phi}^a + m^2\mathbf{L}^-(\mathbf{x}^d)\sum_{a=1}^{n^-}\mathbf{P}_1^a(\mathbf{x})\hat{\phi}^a\\
&-m^2\mathbf{L}^+(\mathbf{x}^d)\sum_{a=1}^{n^+}\mathbf{P}_3^a(\mathbf{x})\hat{\phi}^a + m^2\mathbf{L}^-(\mathbf{x}^d)\sum_{a=1}^{n^-}\mathbf{P}_3^a(\mathbf{x})\hat{\phi}^a\\
&- m^2\mathbf{M}^+(\mathbf{x}^d)\sum_{a=1}^{n^+}\mathbf{P}_1^a(\mathbf{x})\hat{\psi}^a + m^2\mathbf{M}^-(\mathbf{x}^d)\sum_{a=1}^{n^-}\mathbf{P}_1^a(\mathbf{x})\hat{\psi}^a\\
&- m^2\mathbf{M}^+(\mathbf{x}^d)\sum_{a=1}^{n^+}\mathbf{P}_3^a(\mathbf{x})\hat{\psi}^a + m^2\mathbf{M}^-(\mathbf{x}^d)\sum_{a=1}^{n^-}\mathbf{P}_3^a(\mathbf{x})\hat{\psi}^a\\
&+ l^2\mathbf{C}^+(\mathbf{x}^d)\sum_{a=1}^{n^+}\mathbf{B}_1^a(\mathbf{x})\mathbf{u}^a - l^2\mathbf{C}^-(\mathbf{x}^d)\sum_{a=1}^{n^-}\mathbf{B}_1^a(\mathbf{x})\mathbf{u}^a\\
&+l^2\mathbf{C}^+(\mathbf{x}^d)\sum_{a=1}^{n^+}\mathbf{B}_3^a(\mathbf{x})\mathbf{u}^a - l^2\mathbf{C}^-(\mathbf{x}^d)\sum_{a=1}^{n^-}\mathbf{B}_3^a(\mathbf{x})\mathbf{u}^a\Bigg] = 0.
\end{aligned} \tag{57}$$

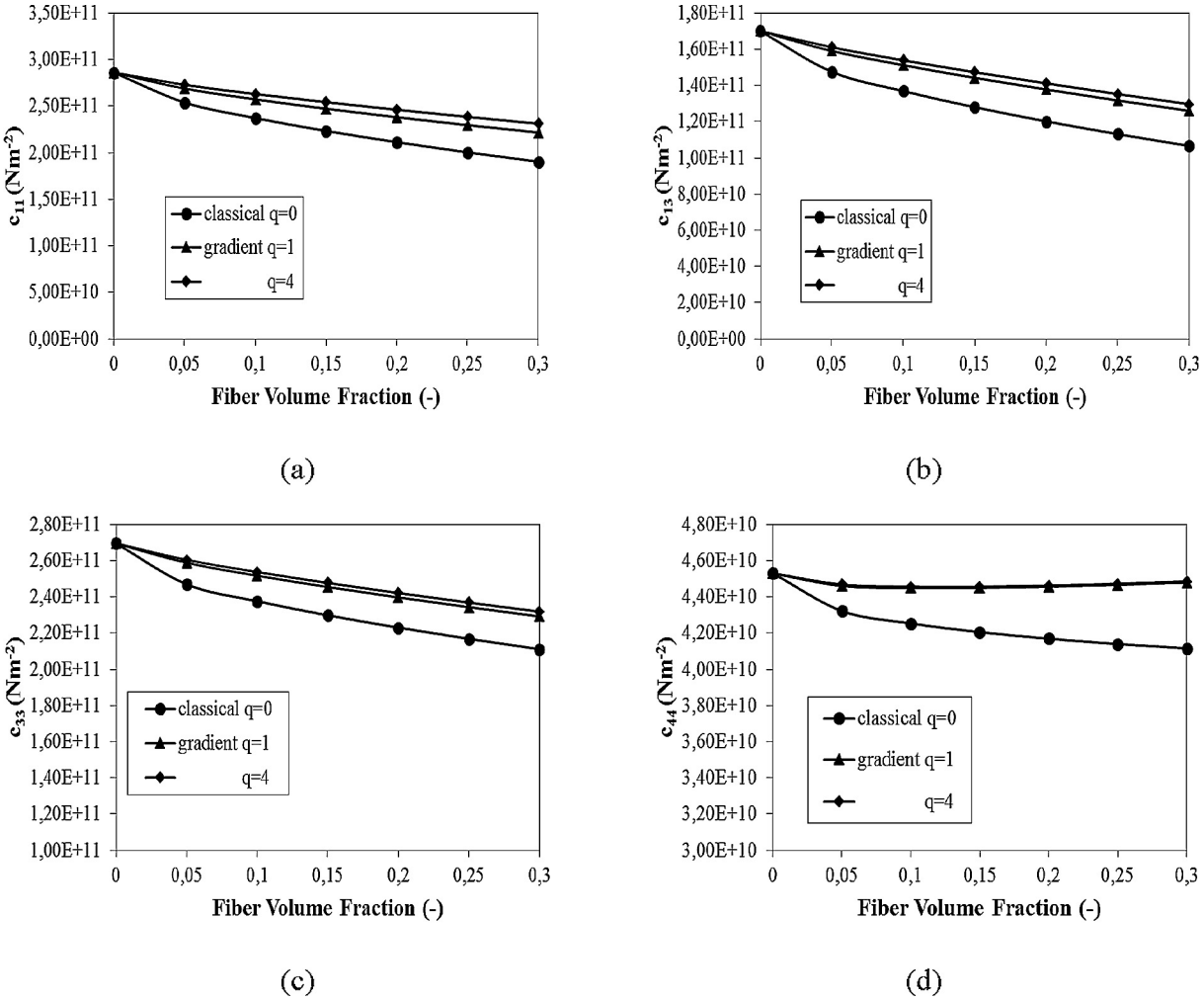

Fig. 4. Variation of effective elastic coefficients with volume fraction of the coated fiber.

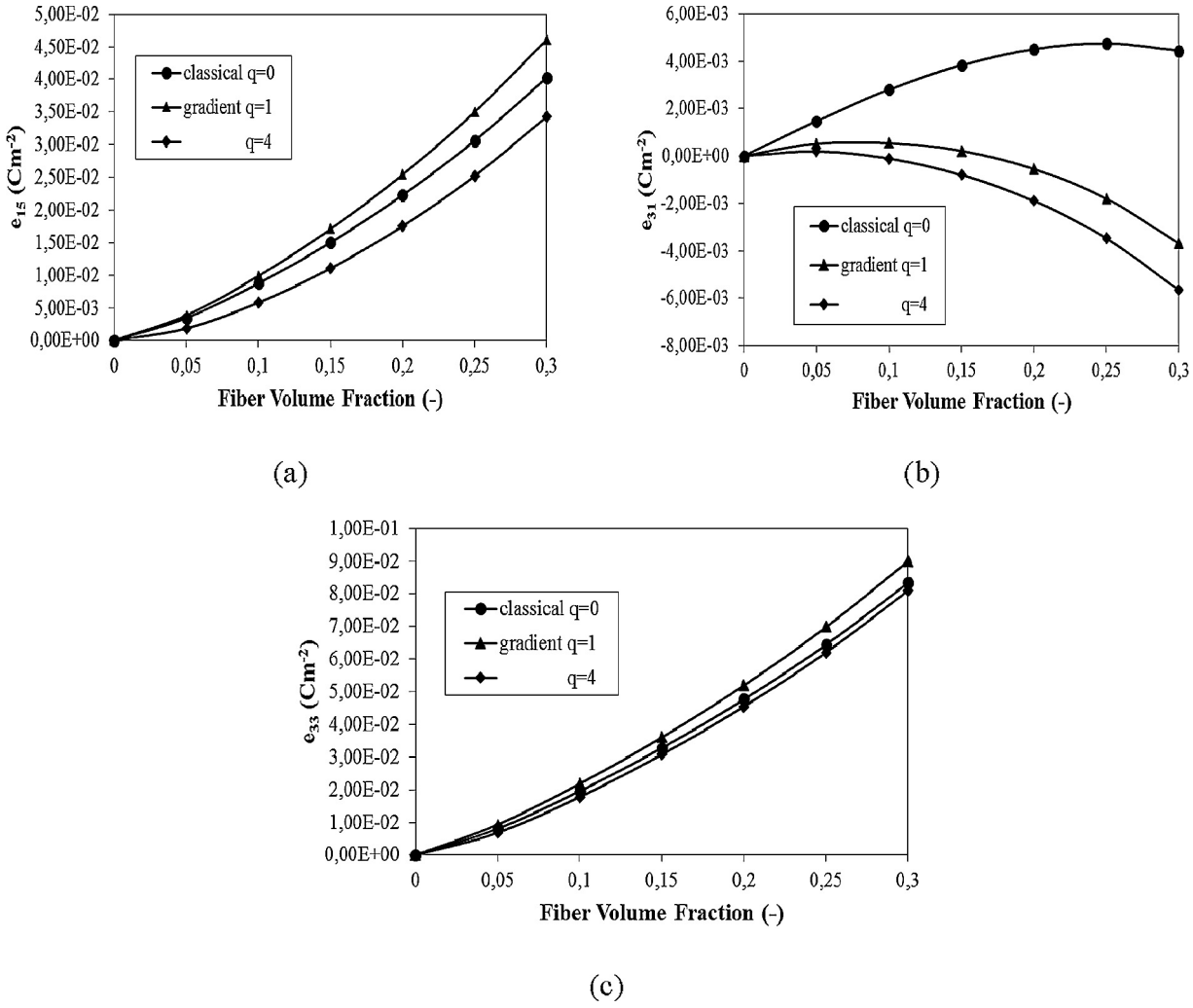

Fig. 5. Variation of effective piezoelectric coefficients with volume fraction of the coated fiber.

$$\mathbf{N}_1(\mathbf{x})\Big[\mathbf{L}^{+T}(\mathbf{x}^d)\sum_{a=1}^{n^+}\mathbf{B}^a(\mathbf{x})\hat{\mathbf{u}}^a-\mathbf{L}^{-T}(\mathbf{x}^d)\sum_{a=1}^{n^-}\mathbf{B}^a(\mathbf{x})\hat{\mathbf{u}}^a+\mathbf{J}^{+}(\mathbf{x}^d)\sum_{a=1}^{n^+}\mathbf{P}^a(\mathbf{x})\hat{\phi}^a$$
$$-\mathbf{J}^{-}(\mathbf{x}^d)\sum_{a=1}^{n^-}\mathbf{P}^a(\mathbf{x})\hat{\phi}^a-\mathbf{A}^{+}(\mathbf{x}^d)\sum_{a=1}^{n^+}\mathbf{P}^a(\mathbf{x})\hat{\psi}^a+\mathbf{A}^{-}(\mathbf{x}^d)\sum_{a=1}^{n^-}\mathbf{P}^a(\mathbf{x})\hat{\psi}^a$$
$$+m^2\mathbf{L}^{+T}(\mathbf{x}^d)\sum_{a=1}^{n^+}\mathbf{B}_4^a(\mathbf{x})\hat{\mathbf{u}}^a-m^2\mathbf{L}^{-T}(\mathbf{x}^d)\sum_{a=1}^{n^-}\mathbf{B}_4^a(\mathbf{x})\hat{\mathbf{u}}^a+$$
$$+m^2\mathbf{L}^{+T}(\mathbf{x}^d)\sum_{a=1}^{n^+}\mathbf{B}_5^a(\mathbf{x})\hat{\mathbf{u}}^a-m^2\mathbf{L}^{-T}(\mathbf{x}^d)\sum_{a=1}^{n^-}\mathbf{B}_5^a(\mathbf{x})\hat{\mathbf{u}}^a\Big]=0, \tag{58}$$

$$\mathbf{N}_1(\mathbf{x}^d)\Big[\mathbf{M}^{+\mathbf{T}}(\mathbf{x}^d)\sum_{a=1}^{n^+}\mathbf{B}^a(\mathbf{x})\hat{\mathbf{u}}^a-\mathbf{M}^{-\mathbf{T}}(\mathbf{x}^d)\sum_{a=1}^{n^-}\mathbf{B}^a(\mathbf{x})\hat{\mathbf{u}}^a-\mathbf{A}^{+}(\mathbf{x}^d)\sum_{a=1}^{n^+}\mathbf{P}^a(\mathbf{x})\hat{\phi}^a$$
$$+\mathbf{A}^{-}(\mathbf{x}^d)\sum_{a=1}^{n^-}\mathbf{P}^a(\mathbf{x})\hat{\phi}^a-\mathbf{I}^{+}(\mathbf{x}^d)\sum_{a=1}^{n^+}\mathbf{P}^a(\mathbf{x})\hat{\psi}^a+\mathbf{I}^{-}(\mathbf{x}^d)\sum_{a=1}^{n^-}\mathbf{P}^a(\mathbf{x})\hat{\psi}^a$$
$$+m^2\mathbf{M}^{+\mathbf{T}}\mathbf{x}^d\sum_{a=1}^{n^+}\mathbf{B}_4^a(\mathbf{x})\hat{\mathbf{u}}^a-m^2\mathbf{M}^{-\mathbf{T}}\mathbf{x}^d\sum_{a=1}^{n^-}\mathbf{B}_4^a(\mathbf{x})\hat{\mathbf{u}}^a$$
$$+m^2\mathbf{M}^{+\mathbf{T}}(\mathbf{x}^d)\sum_{a=1}^{n^+}\mathbf{B}_5^a(\mathbf{x})\hat{\mathbf{u}}^a-m^2\mathbf{M}^{-\mathbf{T}}(\mathbf{x}^d)\sum_{a=1}^{n^-}\mathbf{B}_5^a(\mathbf{x})\hat{\mathbf{u}}^a\Big]=0, \tag{59}$$

where n^+ and n^- are the numbers of nodes lying in the support domain in medium + and medium -, respectively. The normal vector components in $\mathbf{N}(\mathbf{x}^d)$ is taken in the sense of outward normal to the medium +.

It is seen from constitutive equations that strain-gradient piezoelectric model can be reduced to the classical piezoelectric model if the internal length material parameter, l, and scaling parameter, m, appearing in Eqs. (5)–(7) vanish. The classical piezoelectric model has been analyzed in an earlier paper by the authors [21]. To assess the size effect, we can introduce the strain-gradient size-factor, q, as

$$l^2=q\cdot l_0^2,\quad m^2=q\cdot m_0^2, \tag{60}$$

where $m_0=2\times10^{-8}$ m and $l_0=2\times10^{-9}$ m are fixed parameters selected for the present model.

The numerical results for effective elastic material parameters are presented in Fig. 4 for fiber volume fraction values in interval from 0.05 to 0.3. All effective elastic coefficients decrease with growing fiber volume fraction. One can also observe that the effective elastic coefficients increase with increasing strain gradient parameter q, but saturate when q reaches 4. However, this enhancement is not significant due to the small volume fraction of the cladding layer on the whole composite content.

The variation of the effective piezoelectric coefficients with the volume fraction of the coated fiber is presented in Fig. 5. The coefficients e_{15} and e_{33} show an increase with growing fiber volume fraction. It is interesting that the strain gradient produces an oppo-

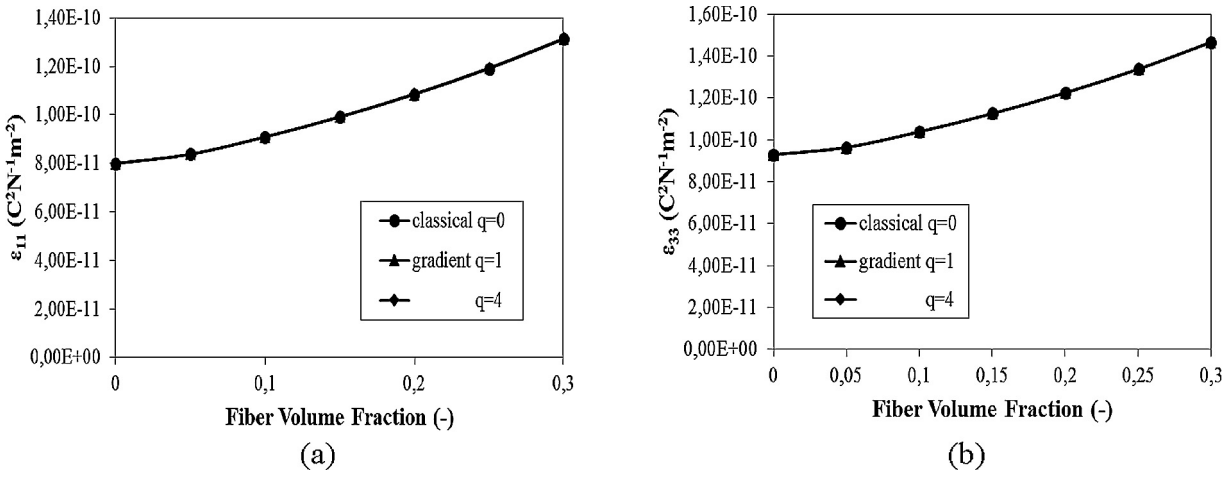

Fig. 6. Variation of effective dielectric permittivities with volume fraction of the coated fiber.

site effect for piezoelectric coefficient e_{31} as compared to the other ones. The positive value is changing to negative with an increase in q. The magnitude of e_{31} is increasing with q. The magnitudes of e_{15} and e_{33} can be tuned by different values of the strain gradient parameter q.

The effective dielectric permittivities, shown in Fig. 6, are increasing as fiber volume fraction increases. One can also observe that for fixed volume fraction, the effective dielectric permittivity is nearly independent of the strain gradient.

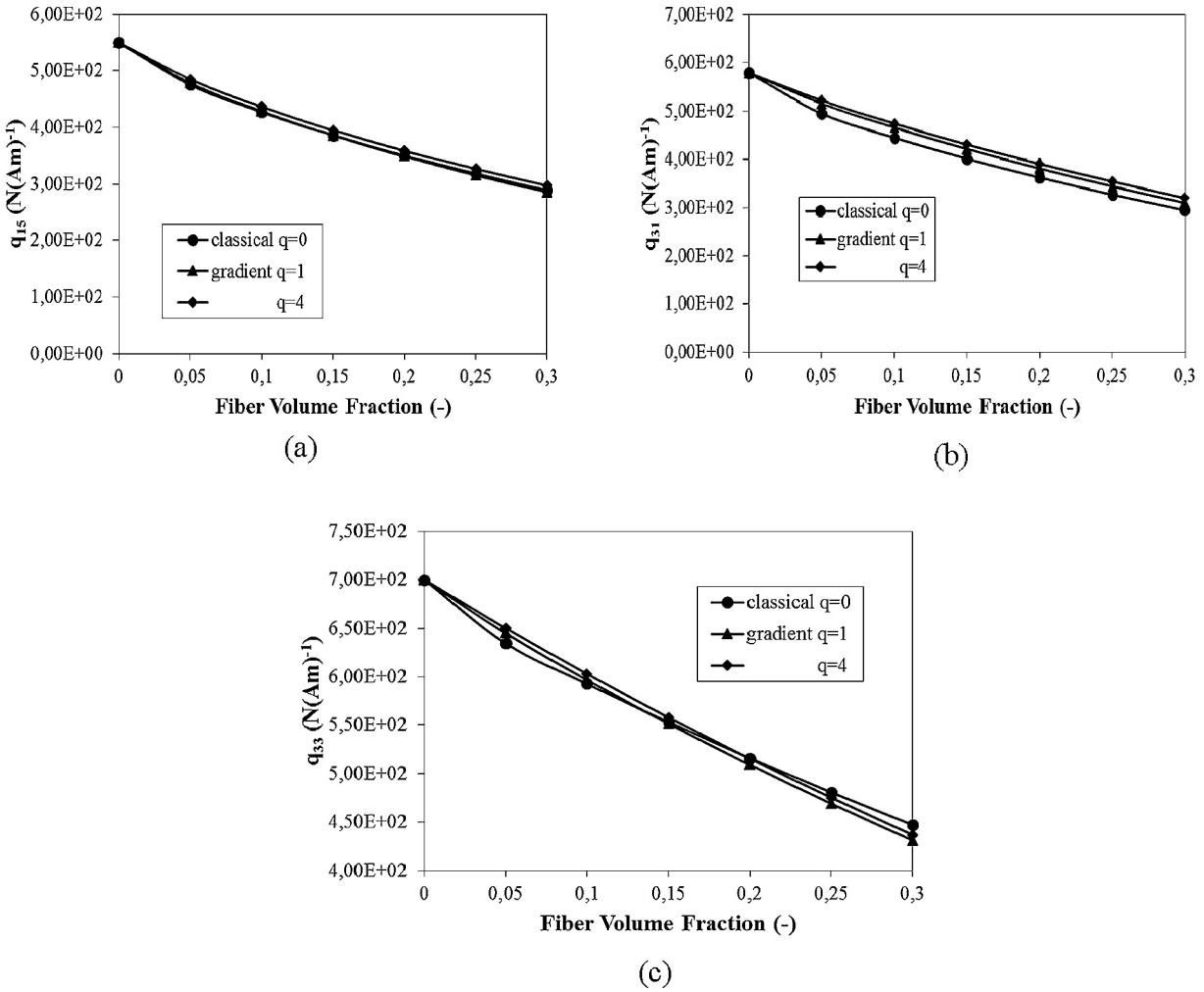

Fig. 7. Variation of effective piezomagnetic coefficients with volume fraction of the coated fiber.

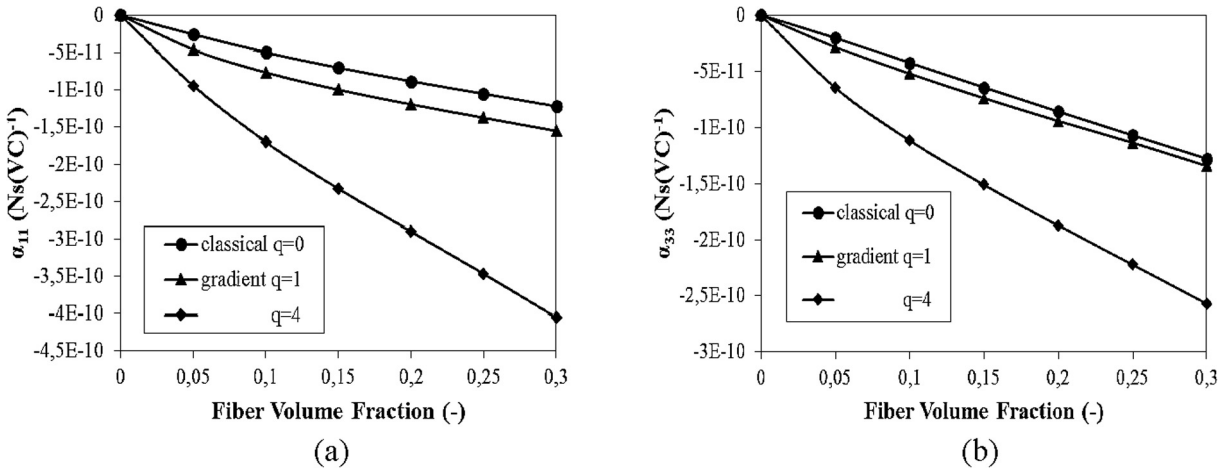

Fig. 8. Variation of effective magnetoelectric coefficients with volume fraction of the coated fiber.

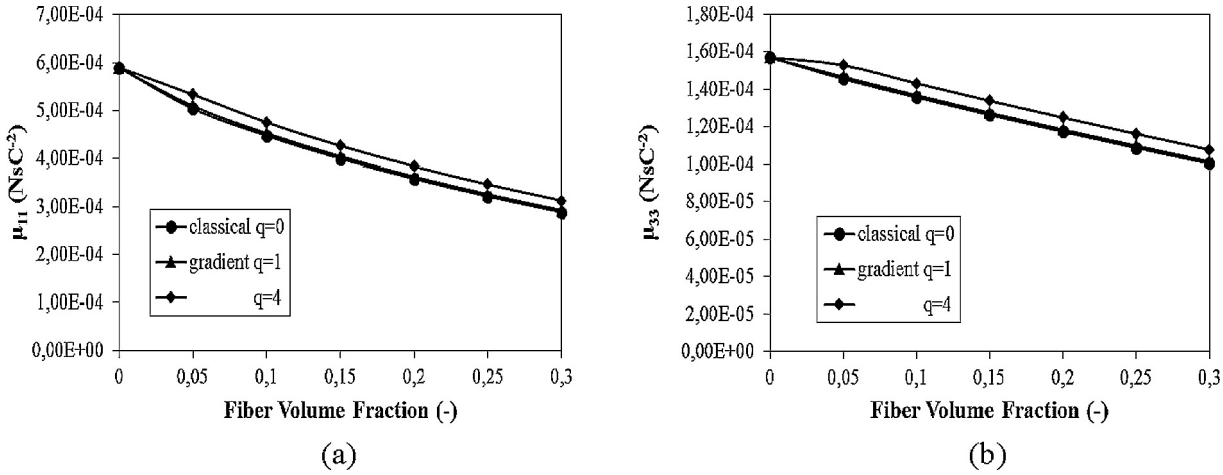

Fig. 9. Variation of effective magnetic permeabilities with volume fraction of the coated fiber.

Variation of the effective piezomagnetic coefficients with the volume fraction of coated fiber is shown in Fig. 7. The effective piezomagnetic coefficients are reduced as the volume fraction of the fiber increases. The effect of strain gradients is insignificant for all effective piezomagnetic coefficients.

Variation of the effective magnetoelectric coefficients with the volume fraction of the coated fiber is shown in Fig. 8. The magnitude of these coefficients highly increases as the fiber volume fraction increases. One can also observe a strong influence of the strain gradient on the effective magnetoelectric coefficients. The effective magnetoelectric coefficients are enhanced as compared to the classical models, particularly when q is large.

Finally, Fig. 9 shows the effect of fiber volume fraction on the effective magnetic permeabilities. Both effective magnetic permeabilities decrease with increasing volume fraction of the coated piezoelectric fiber. The influence of strain gradients on the effective magnetic permeabilities is also very small.

6. Conclusions

A new formulation based on the meshless local Petrov-Galerkin (MLPG) method is developed for the evaluation of the effective material properties in MEE composite materials described by the gradient theory. The strain-gradients are considered in the constitutive equations. The composite is made of a piezomagnetic matrix with embedded piezoelectric fibers with nano-sized coating layer. The governing equations with the corresponding boundary conditions are derived using the variational principle. The local integral equations for the solution of 2D boundary value problems of magnetoelectroelasticity are derived in the gradient theory.

It follows from the numerical analyses that the effective elastic, piezoelectric, magnetoelectric coefficients and magnetic permeabilities are influenced significantly by the strain-gradient. While the effective piezomagnetic coefficients and dielectric permeabilities are influenced very weakly. The strongest influence of the cladding layer is observed in the effective magnetoelectric (ME) coefficients. The influence of the coating layer on the effective ME coefficient is dominant although the ME coefficients for all three composite constituents (fiber, matrix, coating) are zero. Thus, our MLPG modeling results could open an opportunity for enhancing the ME coefficients in coated fiber composites for possible promising future applications.

The strain-gradient theory should be employed if the dimensions of the analyzed problem are of the same order of magnitude as the internal material length. Numerical results illustrate that size-effect phenomenon must be considered in such cases. The MLPG method has been successfully applied to nano-MEE composites. The present local integral equation method requires no fundamental solutions and all integrands in the present formulation are regular. Therefore, the method is promising for numerical analysis

of general multi-field problems with more complex constitutive equations even in the gradient theory.

Acknowledgement

The authors acknowledge the support by the Slovak Science and Technology Assistance Agency registered under number APVV-14-0216 and VEGA-1/0145/16.

References

[1] Avellaneda M, Harshe G. Magnetoelectric effect in piezoelectric/magnetostrictive multilayer (2–2) composites. J Intell Mater Syst Struct 1994;5:501–13.
[2] Nan CW. Magnetoelectric effect in composites of piezoelectric and piezomagnetic phases. Phys Rev B 1994;50:6082–8.
[3] Ryu J, Priya S, Uchino K, Kim HE. Magnetoelectric effect in composites of magnetostrictive and piezoelectric materials. J Electroceram 2002;8:107–19.
[4] Hierold C, Jungen A, Stampfer C, Helbling T. Nano electromechanical sensors based on carbon nanotubes. Sens Actuators A 2007;136:51–61.
[5] Lau KT, Cheung HY, Lu J, Yin YS, Hui D, Li HL. Carbon nanotubes for space and bio-engineering applications. J Comput Theor Nanosci 2008;5:23–35.
[6] Baughman RH, Cui C, Zakhidov AA, Iqbal Z, Barisci JN, Spinks GM, et al. Carbon nanotube actuators. Science 1999;284:1340–4.
[7] Lau KT, Hui D. The revolutionary creation of new advanced materials-carbon nanotube composites. Compos Part B-Eng 2002;33:263–77.
[8] Lau KT, Chipara M, Ling HY, Hui D. On effective elastic moduli of carbon nanotubes for nanocomposite structures. Compos Part B-Eng 2004;35:95–101.
[9] Frankland SJV, Caglar A, Brenner DW, Griebel M. Molecular simulation of the influence of chemical cross-links on the shear strength of carbon nanotube-polymer interfaces. J Phys Chem B 2002;106:3046–8.
[10] Liew KM, He XQ, Wong CH. On the study of elastic and plastic properties of multi-walled carbon nanotubes under axial tension using molecular dynamics simulation. Acta Mater 2004;52:2521–7.
[11] Tang Z, Xu Y, Li G, Aluru NR. Physical models for coupled electromechanical analysis of silicon nanoelectromechanical systems. J Appl Phys 2005;97:114304.
[12] Fleck NA, Muller GM, Ashby MF, Hutchinson JW. Strain gradient plasticity: theory and experiments. Acta Metall Mater 1994;42:475–87.
[13] Lam DCC, Yang F, Chong ACM, Wang J, Tong P. Experiments and theory in strain gradient elasticity. J Mech Phys Solids 2003;51:1477–508.
[14] Li XF, Wang BL, Lee KY. Size effects of the bending stiffness of nanowires. J Appl Phys 2009;105:074306.
[15] Qi Lu, Zhou Shenjie, Li Anqing. Size-dependent bending of an electro-elastic bilayer nanobeam due to flexoelectricity and strain gradient elastic effect. Compos Struct 2016;135:167–75.
[16] Bishay PL, Sladek J, Sladek V, Atluri SN. Analysis of functionally graded multiferroic composites using hybrid/mixed finite elements and node-wise material properties. CMC: Comput Mater Continua 2012;29:213–62.
[17] Kuo HY, Wang YL. Optimization of magnetoelectricity in multiferroic fibrous composites. Mech Mater 2012;50:88–99.
[18] Wang X, Pan E. Magnetoelectric effects in multiferroic fibrous composite with imperfect interface. Phys Rev B 2007;76:214107.
[19] Kuo HY. Multicoated elliptic fibrous composites of piezoelectric and piezomagnetic phases. Int J Eng Sci 2011;49:561–75.
[20] Kuo HY, Pan E. Effective magnetoelectric effect in multicoated circular fibrous multiferroic composites. J Appl Phys 2011;109:104901.
[21] Sladek J, Sladek V, Pan E. Effective properties of coated fiber-composites with piezoelectric and piezomagnetic phases. J Intell Mater Syst Struct 2017;28:97–107.
[22] Ebrahimi Farzad, Dabbagh Ali. On flexural wave propagation responses of smart FG magneto-electroelastic nanoplates via nonlocal strain gradient theory. Compos Struct 2017;162:281–93.
[23] Ohs RR, Aluru NR. Meshless analysis of piezoelectric devices. Comput Mech 2001;27:23–36.
[24] Liu GR, Dai KY, Lim KM, Gu YT. A point interpolation mesh free method for static and frequency analysis of two-dimensional piezoelectric structures. Comput Mech 2002;29:510–9.
[25] Zhu T, Zhang JD, Atluri SN. A local boundary integral equation (LBIE) method in computational mechanics, and a meshless discretization approaches. Comput Mech 1998;21:223–35.
[26] Atluri SN, Sladek J, Sladek V, Zhu T. The local boundary integral equation (LBIE) and its meshless implementation for linear elasticity. Comput Mech 2000;25:180–98.
[27] Sladek J, Stanak P, Han ZD, Sladek V, Atluri SN. Applications of the MLPG method in engineering & Sciences: a review. CMES: Comput Model Eng Sci 2013;92:423–75.
[28] Atluri SN, Han ZD, Shen S. Meshless local Petrov-Galerkin (MLPG) approaches for solving the weakly-singular traction & displacement boundary integral equations. CMES: Comput Model Eng Sci 2003;4:507–16.
[29] Sladek J, Sladek V, Atluri SN. Meshless local Petrov-Galerkin method in anisotropic elasticity. CMES: Comput Model Eng Sci 2004;6:477–89.
[30] Sladek J, Sladek V, Zhang Ch, Schanz M. Meshless local Petrov-Galerkin method for continuously nonhomogeneous linear viscoelastic solids. Comput Mech 2006;37:279–89.
[31] Sladek J, Sladek V, Zhang Ch, Solek P. Application of the MLPG to thermo-piezoelectricity. CMES: Comput Model Eng Sci 2007;22(3):217–33.
[32] Sladek J, Sladek V, Zhang Ch, Solek P, Pan E. Evaluation of fracture parameters in continuously nonhomogeneous piezoelectric solids. Int J Fract 2007;145:313–26.
[33] Sladek J, Sladek V, Solek P, Pan E. Fracture analysis of cracks in magneto-electro-elastic solids by the MLPG. Comput Mech 2008;42:697–714.
[34] Sladek J, Sladek V, Zhang Ch, Wunsche M. Semi-permeable crack analysis in magnetoelectroelastic solids. Smart Mater Struct 2012;21:025003.
[35] Atluri SN. The meshless method (MLPG) for domain and BIE discretizations. Forsyth: Tech Science Press; 2004.
[36] Hu SL, Shen SP. Electric field gradient theory with surface effect for nano-dielectrics. CMC: Comput Mater Continua 2009;13:63–87.
[37] Exadaktylos GE, Vardoulakis I. Microstructure in linear elasticity and scale effects: a reconsideration of basic rock mechanics and rock fracture mechanics. Tectonophysics 2001;335:81–109.
[38] Liang X, Shen S. Size-dependent piezoelectricity and elasticity due to the electric field-strain gradient coupling and strain gradient elasticity. Int J Appl Mech 2013;5:1350015.
[39] Pan E, Chen W. Static Green's functions in anisotropic media. New York: Cambridge University Press; 2015.
[40] Krongauz Y, Belytschko T. EFG approximation with discontinuitous derivatives. Int J Numer Methods Eng 1998;41:1215–33.
[41] Cordes LW, Moran B. Treatment of material discontinuity in the element free Galerkin method. Comput Methods Appl Mech Eng 1996;139:75–89.
[42] Li Q, Shen S, Han ZD, Atluri SN. Application of meshless local Petrov-Galerkin (MLPG) to problems with singularities, and material discontinuities, in 3-D elasticity. CMES: Comput Model Eng Sci 2003;4:571–85.